

Stochastic pH Oscillations in a Model of the Urea–Urease Reaction Confined to Lipid Vesicles

Arthur V. Straube,* Stefanie Winkelmann, Christof Schütte, and Felix Höfling



Cite This: *J. Phys. Chem. Lett.* 2021, 12, 9888–9893



Read Online

ACCESS |



Metrics & More

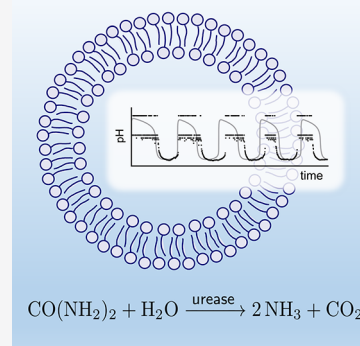


Article Recommendations



Supporting Information

ABSTRACT: The urea–urease clock reaction is a pH switch from acid to basic that can turn into a pH oscillator if it occurs inside a suitable open reactor. We numerically study the confinement of the reaction to lipid vesicles, which permit the exchange with an external reservoir by differential transport, enabling the recovery of the pH level and yielding a constant supply of urea molecules. For microscopically small vesicles, the discreteness of the number of molecules requires a stochastic treatment of the reaction dynamics. Our analysis shows that intrinsic noise induces a significant statistical variation of the oscillation period, which increases as the vesicles become smaller. The mean period, however, is found to be remarkably robust for vesicle sizes down to approximately 200 nm, but the periodicity of the rhythm is gradually destroyed for smaller vesicles. The observed oscillations are explained as a canard-like limit cycle that differs from the wide class of conventional feedback oscillators.



Oscillations are vital for the processes of life, such as metabolism, signaling, cell growth, and cell division,^{1,2} with examples ranging from fast signaling cycles and calcium oscillations to slow circadian rhythms.³ Cells gain control over these processes by biochemical reaction networks,^{4,5} e.g., gene-regulatory, protein-interaction, and metabolic networks, which almost always involve enzyme-catalyzed reactions. Protonation and biprotonation can significantly affect the enzymatic activity, leading to a bell-shaped dependence of the reaction speed upon the H^+ concentration or, equivalently, the pH level.⁶ Such a dependence can give rise to pronounced periodic pH variations, the key driving factor for pH oscillators.⁷ A conventional pH oscillator is built up by balancing a positive, autocatalytic feedback (production of H^+) with a time-delayed, negative feedback (e.g., consumption of products).^{2,7} A qualitatively different pH oscillator has recently been suggested for a lipid vesicle with the urea–urease clock reaction^{8–10} periodically recovered by the differential transport of acid and urea across the vesicle membrane.^{11–13}

Experimentally, urea–urease pH oscillations were observed thus far in macroscopic reaction volumes.^{9,14} Also, most analyses of pH oscillators to date have relied on deterministic reaction rate equations (RREs). Furthermore, there is a growing interest in chemical oscillators for applications.^{15–19} This motivates the question whether stable limit cycles persist and how they change upon downscaling from the macroscopic to, e.g., intracellular reaction volumes. Indeed, the cytoplasm is a highly heterogeneous medium exhibiting macromolecular crowding and compartmentalization, with repercussions on the reaction kinetics.^{20–23} Enzymatic activity is confined to small reaction chambers ranging from about 10 μm for lipid

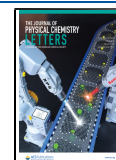
membrane organelles²⁴ down to 20 nm for bacterial micro-compartments^{25,26} and outer membrane vesicles.^{27,28} Such small compartments can host only very limited copy numbers of molecules, necessitating the replacement of RREs by their discrete and inherently stochastic counterparts.^{29–31} Intrinsic noise as a result of such molecular discreteness leads to a breakdown of the macroscopic theory of Michaelis–Menten kinetics.^{32–34} For monostable reaction networks, not only the size of fluctuations^{35,36} but also the mean concentrations^{37,38} become volume-dependent. Furthermore, intrinsic noise may change the stability of steady states, inducing oscillations in deterministic systems without limit cycles,^{39,40} or alter the characteristics of limit cycles.⁴¹ However, its impact on pH-regulated systems has remained largely unexplored.

In this work, we consider the urea–urease reaction and study how the stable rhythmic variation of the pH level^{12,14} is affected by intrinsic noise when decreasing reaction volumes to biologically relevant scales. Within one cycle, molecular copy numbers can vary from a few molecules to several thousands almost instantaneously, which is captured by the stochastic simulations. We detect irregular oscillations, perform a statistical analysis of the period lengths, and gain further insight into the oscillation mechanism.

Received: September 13, 2021

Accepted: September 30, 2021

Published: October 5, 2021



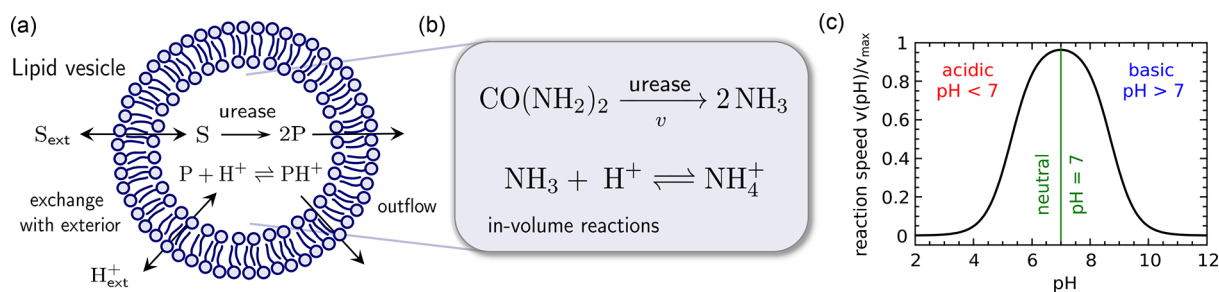


Figure 1. Schematic representation of the enzyme-assisted reaction network. (a) Enzyme (urease) catalyzes conversion of the substrate (urea) into product (ammonia) in a lipid vesicle compartment affected by changing acidity (hydrogen ion, H^+). The products (ammonia and ammonium) are subjected to decay or outflow from the vesicle, while the substrate and acid exchange with the exterior of the vesicle. (b) Volume reactions **1a** and **1b** taking place in the vesicle, showing the meaning of the involved components; H_2O and CO_2 have been omitted in the first reaction. (c) Reaction speed $\nu = k_{\text{cat}}([S], [H^+])[S]$ of the catalytic step (reaction **1a**) evaluated for urease (see eq 2) shows a strong dependence upon the level of $pH = -\log_{10}([H^+]/1 \text{ M})$; it is fastest in a neutral medium ($pH \approx 7$).

Our study is based on a minimal model for the urease-catalyzed urea hydrolysis, which exhibits pH oscillations while admitting a simple representation as a reaction network to facilitate the stochastic simulations. Bánsági and Taylor¹¹ showed that the full model of the urea–urease reaction cycle, involving the concentrations of eight molecular species, can be reduced to an effective five-variable model. To further simplify, we eliminate one more species (OH^-) from the reaction network with merely small quantitative changes to the evolution of the remaining concentrations (see the Supporting Information). The corresponding reaction scheme involves only four species and consists of two core reactions that are assumed to take place inside a lipid vesicle, serving as a small-size, well-mixed reaction compartment of volume V . In addition, the vesicle can exchange molecules with its exterior via a permeable membrane (Figure 1a). Under the action of urease enzymes, urea $CO(NH_2)_2$ as the substrate species S is converted into ammonia molecules NH_3 as product P (Figure 1b). Concomitantly, ammonia reacts with the acid to form ammonium ions (abbreviated as PH^+ in the following). Thus, the reactions inside the vesicle read as follows:



The speed of reaction **1a** is crucially affected by the acidity of the medium and controlled by the available amount X_{H^+} of protons H^+ ; the proton concentration $[H^+] = X_{H^+}/V_M$ is converted to the pH value via $pH = -\log_{10}([H^+]/1 \text{ M})$ in terms of the molar volume $V_M = VN_A$ and Avogadro's number N_A . Hereafter, we denote the numbers of molecules of species S , H^+ , P , and PH^+ as X_S , X_{H^+} , X_P , X_{PH^+} , respectively; we will reserve square brackets to refer to concentrations, namely, $[S] = X_S/V_M$, etc.

The efficacy of the catalytic step (reaction **1a**) is modeled by an effective rate^{6,11,42}

$$k_{\text{cat}}([S], [H^+]) = \frac{k_{\text{cat}}^M([S])}{1 + [H^+]/K_{E1} + K_{E2}/[H^+]} \quad (2)$$

with the conventional Michaelis–Menten rate in the absence of pH effects given by

$$k_{\text{cat}}^M([S]) = \frac{\nu_{\text{max}}}{K_M + [S]} \quad (3)$$

and the Michaelis–Menten constant^{9,11,43} $K_M = 3 \times 10^{-3} \text{ M}$. The rate $k_{\text{cat}}([S], [H^+])$ possesses a maximum that is proportional to ν_{max} at an optimal amount of H^+ , and reaction **1a** is suppressed for H^+ concentrations smaller and larger than this value or equivalently at large and small pH values, as determined by the constants^{9,11,43} $K_{E1} = 5 \times 10^{-6} \text{ M}$ and $K_{E2} = 2 \times 10^{-9} \text{ M}$ (see Figure 1c). For the stochastic simulations in terms of particle numbers X_S , we evaluate $k_{\text{cat}}(X_S/V_M, X_{H^+}/V_M)$ as the propensity for reaction **1a** to occur. This reaction is further coupled to reaction **1b**, meaning that the product is also affected by the acidity and can reversibly turn into ammonium ions PH^+ . The corresponding rates are set as^{9,11,44} $k_2 = 4.3 \times 10^{10} \text{ M}^{-1} \text{ s}^{-1}$ and $k_{2r} = 24 \text{ s}^{-1}$.

Apart from the in-volume reactions **1a** and **1b**, we assume outflow or decay of the product in both of its forms, P and PH^+ , with the rate constant $k > 0$. Further, we consider an explicit exchange of S and H^+ with the exterior of the vesicle serving as a reservoir, with rates k_S and k_H , respectively, equal in both directions. The spatial exchange between the interior and exterior of the vesicle is modeled as the stochastic jump process along the lines of the spatiotemporal master equation^{45,46} and can be written as reactive transitions. Thus, the interaction with the exterior of the reaction volume is summarized as



We treat the reservoir as sufficiently large, such that reactions **4b** lead only to marginal changes to the amounts of S_{ext} and H^+_{ext} . Therefore, we approximate their concentrations by fixed values $[S_{\text{ext}}]$ and $[H^+_{\text{ext}}]$ and replace reactions **4b** by



To inspect oscillatory regimes, we rely on the parameters that were shown to exhibit periodic deterministic oscillations for the urease-loaded membrane.¹¹ Generally, the rate of proton transport k_H should be faster than that of urea k_S ; here, we use $k_H = 9 \times 10^{-3} \text{ s}^{-1}$ and $k_S = 1.4 \times 10^{-3} \text{ s}^{-1}$. The outflow rate of the products is set to $k = k_S$, and the maximum speed is set to $\nu_{\text{max}} = 1.85 \times 10^{-4} \text{ M s}^{-1}$, where the latter corresponds to an urease solution with a catalytic enzyme activity of 50 units ($\mu\text{mol}/\text{min}$). In all simulations, the external values of X_S and X_{H^+} were fixed to match the concentrations $[S_{\text{ext}}] = 3.8 \times$

10^{-4} M and $[H^+_{\text{ext}}] = 1.3 \times 10^{-4}$ M or equivalently to an acidic environment at pH 3.9. Inside of the vesicle, the initial values of X_S and X_{H^+} were chosen to correspond to concentrations $[S]_0 = 5 \times 10^{-5}$ M and $[H^+]_0 = 1 \times 10^{-5}$ M (or pH 5), respectively.

The deterministic evolution of the macroscopic concentrations obeys the RREs of the four-species model (see eqs S1a–S1d of the Supporting Information). For the parameter values chosen above, the results from numerical integration are quantitatively similar to the earlier findings within the five-variable model.¹¹ For an exemplary vesicle size of 250 nm in diameter (i.e., a reaction volume of $V = 8.18 \times 10^{-18}$ L), the evolution of all variables after a short transient displays clear periodic oscillations (solid lines in Figure 2). Especially, the

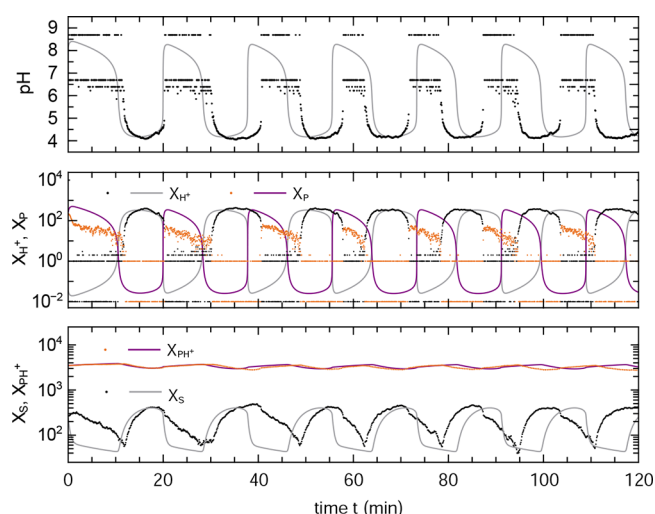


Figure 2. Stochastic evolution of molecule numbers. The pH level (upper panel) and molecule numbers for the species H^+ and P (middle panel) and S and PH^+ (bottom panel) as functions of time for the urea-urease reaction scheme [Figure 1 and eqs 1–5] confined to a vesicle of 250 nm in diameter, which corresponds to a reaction volume of $V = 8.18 \times 10^{-18}$ L. Note the logarithmic scales. Solid lines are solutions to the deterministic reaction rate equations (eqs S1a–S1d of the Supporting Information). Dots show an exemplary solution to the stochastic reaction dynamics obtained with Gillespie's stochastic simulation algorithm;⁴⁷ the special value $X_{H^+} = 0$ is represented as 0.01 (pH \approx 8.7).

pH level varies strongly between pH \approx 4.2 and pH \approx 8.3 (upper panel). Correspondingly, the copy number of protons $X_{H^+} = [H^+]V_M$ (as rescaled solution of the RREs) on a logarithmic scale mirrors this behavior, and the product X_P evolves in antiphase relative to X_{H^+} , with both quantities changing over 4 orders of magnitude rapidly (middle panel). The values of X_{PH^+} show comparably little variation and remain large and distinctly greater than those of the other species (bottom panel). The maximum copy numbers of X_P and X_{H^+} are similar in magnitude to the typical values for the substrate S, while the minima of X_P and X_{H^+} correspond formally to average copy numbers of the order 10^{-2} . Although such values are not prohibited by the reaction rate formalism, the actual copy numbers must be integers, with the closest allowed values being either 0 or 1. This inconsistency is a signature of the deficiency of the macroscopic description at such a small scale.

Stochastic simulations of reactions 1, 4a, and 5 were performed by the stochastic simulation algorithm.^{47,48} In the macroscopic limit of a large reaction volume (e.g., for giant vesicles with a diameter of $10 \mu\text{m}$), the stochastic concentrations converge to the solution of the deterministic RREs given by eqs S1 of the Supporting Information, as expected.^{31,48} With a decreasing volume, the role of intrinsic noise grows and one anticipates deviations from the deterministic description. The stochastic trajectories develop well-pronounced fluctuations and differ significantly from the corresponding deterministic solutions, as demonstrated for a vesicle size of 250 nm in Figure 2. These stochastic effects are weaker for species of a large copy number, e.g., PH^+ , while they are strong for the acid and product, whose amounts drop to a few molecules and even become 0 frequently. The same features are reflected in the oscillations of the pH level, which directly follows from X_{H^+} .

We stress that the intrinsic noise perturbs the rhythm of the pH variation. The stochastic oscillations become clearly irregular from time to time, showing either longer or shorter periods compared to their strictly regular deterministic counterparts. To characterize this kind of stochasticity, we have extracted the period lengths T from a single, long trajectory of X_{H^+} covering about 1500 periods. The obtained sequence of T values shows a high variability (Figure 3a) around the mean period of $T_{\text{av}} = 17.46 \pm 0.06$ min, which is slightly shorter than the value predicted by the deterministic

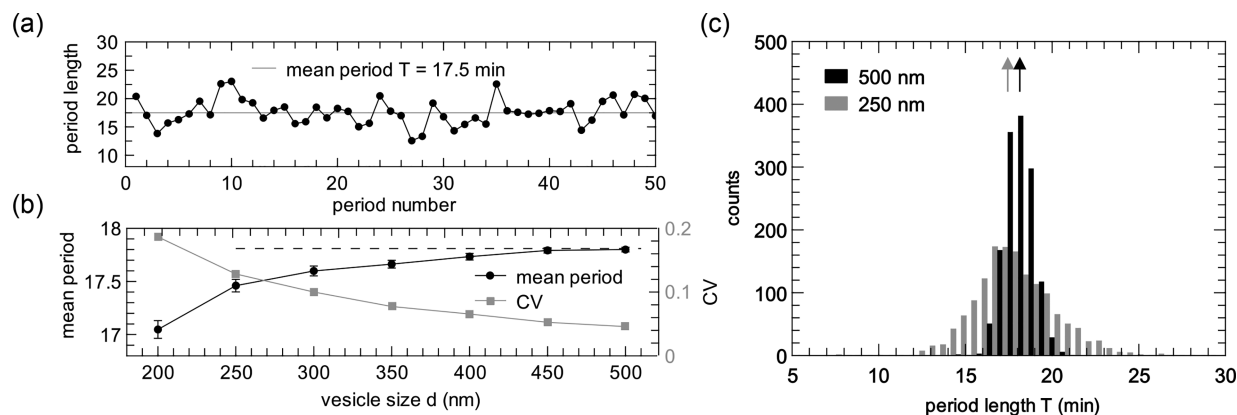


Figure 3. Time periods and their statistical characteristics. (a) Sequence of period lengths (dots) for a vesicle size of 250 nm (reaction volume $V = 8.18 \times 10^{-18}$ L) with the mean over 1500 periods (horizontal line). (b) Mean periods with their statistical errors (disks and bars) and coefficient of variation (CV, squares) for different vesicle sizes. The dashed line indicates the macroscopic value of the period length, $T_{\text{det}} = 17.8$ min. (c) Histogram of the period lengths for vesicle sizes of 500 and 250 nm; arrows indicate the mean periods.

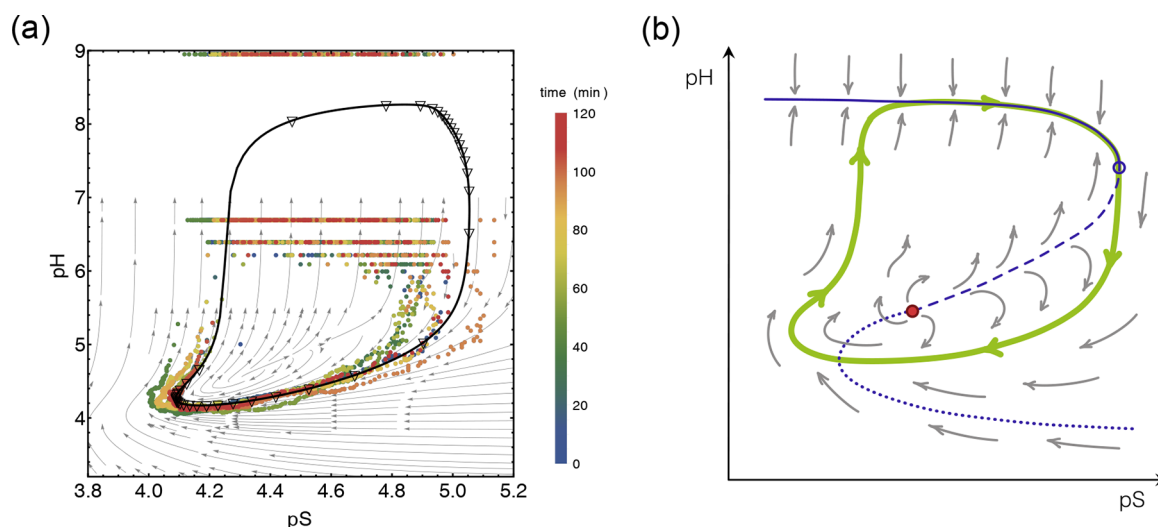


Figure 4. Phase portrait and limit cycle in the pS–pH plane. (a) Limit cycle from the deterministic model (solid line) and stochastic simulations (dots) with $pS = -\log_{10}(X_S/V_M)$. Stochastic results are for a vesicle size of 250 nm and cover six oscillation periods (same data as in Figure 2); data points with $X_{H^+} = 0$ are drawn at the upper frame border, and colors encode time. Open triangles along the limit cycle are equally spaced in time and indicate the speed along the cycle (clockwise); their distribution reflects the alternating phases of fast and slow motion. Gray arrows depict the flow of the dynamic system, obtained approximately for a reduced, two-variable model (see the main text). (b) Structure of the flow and the limit cycle (thick green line) emerge from the combination of an unstable focus (solid, red circle) and canard-type behavior. The latter is determined by the pH nullcline (purple line), where $d[H^+]/dt = 0$, which consists of an attractive branch (solid line), passing through a turning point (open circle) to a repelling (dashed line) and neutrally stable (dotted line) branch. Gray arrows indicate the direction of the phase flow.

model, $T_{\text{det}} = 17.79 \pm 0.01$ min. Further, the data show no sign of a temporal trend in the period length, and an autocorrelation analysis suggests that the lengths of subsequent periods are independent. The large scatter of period lengths along a stochastic trajectory is evidenced from their statistical distribution, shown in Figure 3c for vesicle sizes of 250 and 500 nm. The scatter is larger for the smaller vesicle, and we infer a small shift of the mean value. Indeed, Figure 3b corroborates that the mean oscillation period becomes monotonically shorter upon decreasing the size of the vesicle. At the same time, the coefficient of variation (CV), which is the dimensionless ratio of the standard deviation over the mean, gradually grows for smaller reaction volumes (see Figure 3b). At large volumes, CV tends to 0 as required by the macroscopic limit; for the smallest vesicle size shown (200 nm), we have $CV \approx 0.2$. Generally, this trend is expected because smaller reaction volumes correspond to more discrete and, therefore, more noisy systems. Overall, with the decrease in volume, the oscillations become more and more irregular. For very small vesicles (e.g., 100 nm; see Figure S1 of the Supporting Information), the size of fluctuations becomes comparable to the oscillation amplitude and the periodic oscillatory behavior breaks down.

For a dynamic system showing regular oscillations, the deterministic solution (after an initial transient) follows a limit cycle, i.e., an attractive, closed orbit in the space of concentrations. For the four-variable model studied here, Figure 4a shows the deterministic limit cycle (solid line) in the pS–pH plane, where $pS = -\log_{10}(X_S/V_M)$, overlaid with a short exemplary stochastic trajectory (dots). In this representation, the cycle is followed clockwise. We infer that intrinsic noise causes pronounced irregularities of the stochastic loop, with the trajectory points distributed well around the deterministic cycle for the smaller values of pH (high X_{H^+}) but significantly deviating from it for larger pH (low X_{H^+}). The latter is due to the fact that non-integer copy

numbers are not permitted in the stochastic simulation. The discreteness of the number of protons X_{H^+} is apparent in the figure for $pH \gtrsim 6$ and incompatible with the deterministic solution, which implies $0 < X_{H^+} < 1$ for $pH \gtrsim 7$ for the chosen reaction volume. Thus, the lowest possible values of X_{H^+} either undershoot ($X_{H^+} = 1$) or overshoot ($X_{H^+} = 0$, i.e., formally $pH = \infty$) the upper branch of the deterministic limit cycle.

Further insight into the oscillation mechanism is gained by studying the structure of the deterministic flow (stream lines in Figure 4a). Because such a flow map is non-trivial to obtain for a system of more than two variables, we have approximately reduced the four-variable RRE system to a two-dimensional dynamic system, by resorting to the quasi-steady-state assumptions⁴⁹ for the products P and PH^+ . This *ad hoc* simplification preserves the fixed points of the original system and captures the qualitative structure of the flow; in particular, it yields a limit cycle quantitatively close to that of the full model for $pH \lesssim 6.5$. The closed-loop attractor results from the interplay of an unstable focus point at $(pS, pH) \approx (4.31, 4.57)$, which is the only fixed point, and a canard-type behavior^{50,51} at high pH values. This combination leads to an oscillator motif that differs from standard pictures typical of chemical feedback oscillators^{2,7,52} (Figure 4b).

Typical for canard-type behavior is a coupling between fast and slow dynamics. As depicted in Figure 4b, the upper branch of the pH nullcline (i.e., the manifold $d[H^+]/dt = 0$) is strongly attractive (solid line) and combines fast, almost transverse motion toward the limit cycle orbit followed by the creeping along it (pS increases), which holds until the turning point (open circle) is reached. At this point, the nullcline bends back accompanied by a change of stability: the manifold between the turning point and the fixed point (red circle) is unstable (dashed line) and locally separates the flow into regions of increasing and decreasing pH level. In contrast to toy models for canard dynamics, where the dynamics switches between two attractive branches, the rest of the nullcline in the present

system is neutrally stable (dotted line) and has no obvious effect on the flow structure. Thus, after the turning point is reached, the pH level decreases quickly and the phase trajectory follows the flow set between the repelling manifold and the outer flow field around the unstable focus until the loop is closed. For the stochastic trajectories, which traverse the interior of the limit cycle, we infer that different crossing points of the separatrix lead to a scatter in the phase plane (near $pS \approx 4.8\text{--}5.1$), which explains the observed variability in the period length.

In conclusion, we have studied the urea–urease reaction confined to a nanosized lipid vesicle, which presents a typical clock reaction⁸ effectively raising the pH level. Under suitable conditions, the clock recovers as a result of the exchange of acid and urea with an external reservoir, leading to a pH oscillator that differs from the wide class of conventional feedback oscillators;⁷ instead, it resembles a canard dynamics.^{50,51} The insight gained into the oscillation mechanism can help to optimize experimental setups and design chemical oscillators based on the same principles.

The presented stochastic analysis, in contrast to deterministic studies, shows that intrinsic noise induces a significant statistical variation of the oscillation period, which increases upon downscaling the vesicle size. We note that, although the mean period is remarkably robust for intermediate vesicle sizes, it slightly changes with the vesicle size. Therefore and because of the inevitable size disparity in vesicle suspensions,¹² different oscillators possess slightly detuned eigenfrequencies, an important issue for understanding intervesicle communication and synchronization of rhythms,^{53–55} which would not be captured by deterministic models. Finally, our findings suggest that below a certain scale, which may still be relevant for applications, the periodicity of the rhythm is gradually destroyed. Namely, apart from the irregularity in the period length, strong deviations appear in the oscillation amplitude masked by fluctuations growing with the decrease in the vesicle size. It is likely that similar trends take place for other pH oscillators, which can be answered by specific tests along the lines presented here.

■ ASSOCIATED CONTENT

Supporting Information

The Supporting Information is available free of charge at <https://pubs.acs.org/doi/10.1021/acs.jpcllett.1c03016>.

Deterministic four-variable model corresponding to reactions 1, 4a, and 5 and a figure showing stochastic evolution of molecule numbers for a 100 nm vesicle (PDF)

■ AUTHOR INFORMATION

Corresponding Author

Arthur V. Straube – Zuse Institute Berlin, 14195 Berlin, Germany; orcid.org/0000-0002-8993-017X;
Email: straube@zib.de

Authors

Stefanie Winkelmann – Zuse Institute Berlin, 14195 Berlin, Germany

Christof Schütte – Zuse Institute Berlin, 14195 Berlin, Germany; Freie Universität Berlin, Department of Mathematics and Computer Science, 14195 Berlin, Germany

Felix Höfling – Freie Universität Berlin, Department of Mathematics and Computer Science, 14195 Berlin, Germany; Zuse Institute Berlin, 14195 Berlin, Germany; orcid.org/0000-0002-5961-132X

Complete contact information is available at:
<https://pubs.acs.org/10.1021/acs.jpcllett.1c03016>

Notes

The authors declare no competing financial interest.

■ ACKNOWLEDGMENTS

The authors thank Tamás Bánsági and Federico Rossi for clarifying details of the models in refs 11 and 13. This research has been supported by Deutsche Forschungsgemeinschaft (DFG) through Grant SFB 1114, Project 235221301 (Subproject C03) and under Germany's Excellence Strategy–MATH+: The Berlin Mathematics Research Center (EXC-2046/1), Project 390685689 (Subproject AA1-1).

■ REFERENCES

- (1) Goldbeter, A. *Biochemical Oscillations and Cellular Rhythms*; Cambridge University Press: Cambridge, U.K., 1996; DOI: [10.1017/CBO9780511608193](https://doi.org/10.1017/CBO9780511608193).
- (2) Novák, B.; Tyson, J. J. Design Principles of Biochemical Oscillators. *Nat. Rev. Mol. Cell Biol.* **2008**, *9*, 981–991.
- (3) Panda, S.; Hogenesch, J. B.; Kay, S. A. Circadian Rhythms From Flies to Human. *Nature* **2002**, *417*, 329–335.
- (4) Tyson, J. J.; Chen, K. C.; Novak, B. Sniffers, Buzzers, Toggles and Blinkers: Dynamics of Regulatory and Signaling Pathways in the Cell. *Curr. Opin. Cell Biol.* **2003**, *15*, 221–231.
- (5) Alon, U. *An Introduction to Systems Biology: Design Principles of Biological Circuits*, 2nd ed.; Chapman and Hall/CRC Press (Taylor & Francis Group): Boca Raton, FL, 2019; DOI: [10.1201/9780429283321](https://doi.org/10.1201/9780429283321).
- (6) Alberty, R. A.; Massey, V. On the Interpretation of the pH Variation of the Maximum Initial Velocity of an Enzyme-Catalyzed Reaction. *Biochim. Biophys. Acta* **1954**, *13*, 347–353.
- (7) Orbán, M.; Kurin-Csörgei, K.; Epstein, I. R. pH-Regulated Chemical Oscillators. *Acc. Chem. Res.* **2015**, *48*, 593–601.
- (8) Lente, G.; Bazsa, G.; Fábrián, I. What is and What isn't a Clock Reaction? *New J. Chem.* **2007**, *31*, 1707–1707A.
- (9) Hu, G.; Pojman, J. A.; Scott, S. K.; Wrobel, M. M.; Taylor, A. F. Base-Catalyzed Feedback in the Urea-Urease Reaction. *J. Phys. Chem. B* **2010**, *114*, 14059–14063.
- (10) Bubanja, I. N.; Bánsági, T.; Taylor, A. F. Kinetics of the Urea-Urease Clock Reaction With Urease Immobilized in Hydrogel Beads. *React. Kinet. Mech. Catal.* **2018**, *123*, 177–185.
- (11) Bánsági, T.; Taylor, A. F. Role of Differential Transport in an Oscillatory Enzyme Reaction. *J. Phys. Chem. B* **2014**, *118*, 6092–6097.
- (12) Miele, Y.; Bánsági, T.; Taylor, A. F.; Stano, P.; Rossi, F. Engineering Enzyme-Driven Dynamic Behaviour in Lipid Vesicles. In *Advances in Artificial Life, Evolutionary Computation and Systems Chemistry*; Rossi, F., Mavelli, F., Stano, P., Caivano, D., Eds.; Springer: Cham, Switzerland, 2016; WIVACE 2015. Communications in Computer and Information Science, Vol. 587, pp 197–208, DOI: [10.1007/978-3-319-32695-5_18](https://doi.org/10.1007/978-3-319-32695-5_18).
- (13) Miele, Y.; Bánsági, T.; Taylor, A. F.; Rossi, F. Modelling Approach to Enzymatic pH Oscillators in Giant Lipid Vesicles. In *Advances in Bionanomaterials*; Piotto, S., Rossi, F., Concilio, S., Reverchon, E., Cattaneo, G., Eds.; Springer: Cham, Switzerland, 2018; Lecture Notes in Bioengineering, pp 63–74, DOI: [10.1007/978-3-319-62027-5_6](https://doi.org/10.1007/978-3-319-62027-5_6).
- (14) Muzika, F.; Růžička, M.; Schreiberová, L.; Schreiber, I. Oscillations of pH in the Urea–Urease System in a Membrane Reactor. *Phys. Chem. Chem. Phys.* **2019**, *21*, 8619–8622.

- (15) Cupić, Ž. D.; Taylor, A. F.; Horváth, D.; Orlik, M.; Epstein, I. R. Editorial: Advances in Oscillating Reactions. *Front. Chem.* **2021**, *9*, 690699.
- (16) Shklyaev, O. E.; Yashin, V. V.; Balazs, A. C. Effects of an Imposed Flow on Chemical Oscillations Generated by Enzymatic Reactions. *Front. Chem.* **2020**, *8*, 618.
- (17) Maria, G. Silico Determination of Some Conditions Leading to Glycolytic Oscillations and Their Interference with Some Other Processes in *E. coli* Cells. *Front. Chem.* **2020**, *8*, 526679.
- (18) Budroni, M. A.; Torbensen, K.; Pantani, O. L.; Ristori, S.; Rossi, F.; Abou-Hassan, A. Microfluidic Compartmentalization of Diffusively Coupled Oscillators in Multisomes Induces a Novel Synchronization Scenario. *Chem. Commun.* **2020**, *56*, 11771–11774.
- (19) Mallphanov, I. L.; Vanag, V. K. Distance Dependent Types of Coupling of Chemical Micro-Oscillators Immersed in a Water-in-Oil Microemulsion. *Phys. Chem. Chem. Phys.* **2021**, *23*, 9130–9138.
- (20) Höfling, F.; Franosch, T. Anomalous Transport in the Crowded World of Biological Cells. *Rep. Prog. Phys.* **2013**, *76*, 046602.
- (21) Weiss, M. Crowding, Diffusion, and Biochemical Reactions. In *New Models of the Cell Nucleus: Crowding, Entropic Forces, Phase Separation, and Fractals*; Hancock, R., Jeon, K. W., Eds.; Academic Press: Amsterdam, Netherlands, 2014; International Review of Cell and Molecular Biology, Vol. 307, Chapter 11, pp 383–417, DOI: 10.1016/B978-0-12-800046-5.00011-4.
- (22) Schneider, S. H.; Lockwood, S. P.; Hargreaves, D. I.; Slade, D. J.; LoConte, M. A.; Logan, B. E.; McLaughlin, E. E.; Conroy, M. J.; Slade, K. M. Slowed Diffusion and Excluded Volume Both Contribute to the Effects of Macromolecular Crowding on Alcohol Dehydrogenase Steady-State Kinetics. *Biochemistry* **2015**, *54*, 5898–5906.
- (23) Tsiapalis, D.; Zeugolis, D. I. It is Time to Crowd Your Cell Culture Media – Physicochemical Considerations With Biological Consequences. *Biomaterials* **2021**, *275*, 120943.
- (24) Cooper, G. M.; Hausman, R. E. *The Cell: A Molecular Approach*, 5th ed.; ASM Press: Washington, D.C., 2009.
- (25) Sutter, M.; Boehringer, D.; Gutmann, S.; Günther, S.; Prangishvili, D.; Loessner, M. J.; Stetter, K. O.; Weber-Ban, E.; Ban, N. Structural Basis of Enzyme Encapsulation Into a Bacterial Nanocompartment. *Nat. Struct. Mol. Biol.* **2008**, *15*, 939–947.
- (26) Kerfeld, C. A.; Heinhorst, S.; Cannon, G. C. Bacterial Microcompartments. *Annu. Rev. Microbiol.* **2010**, *64*, 391–408.
- (27) Kaparakis-Liaskos, M.; Ferrero, R. L. Immune Modulation by Bacterial Outer Membrane Vesicles. *Nat. Rev. Immunol.* **2015**, *15*, 375–387.
- (28) Schwechheimer, C.; Kuehn, M. J. Outer-Membrane Vesicles From Gram-Negative Bacteria: Biogenesis and Functions. *Nat. Rev. Microbiol.* **2015**, *13*, 605–619.
- (29) Grima, R.; Schnell, S. Modelling Reaction Kinetics Inside Cells. *Essays Biochem.* **2008**, *45*, 41–56.
- (30) Wilkinson, D. J. Stochastic Modelling for Quantitative Description of Heterogeneous Biological Systems. *Nat. Rev. Genet.* **2009**, *10*, 122–133.
- (31) Winkelmann, S.; Schütte, C. *Stochastic Dynamics in Computational Biology*; Springer: Cham, Switzerland, 2020; Frontiers in Applied Dynamical Systems: Reviews and Tutorials, DOI: 10.1007/978-3-030-62387-6.
- (32) Stefanini, M. O.; McKane, A. J.; Newman, T. J. Single Enzyme Pathways and Substrate Fluctuations. *Nonlinearity* **2005**, *18*, 1575–1595.
- (33) Grima, R. Noise-Induced Breakdown of the Michaelis-Menten Equation in Steady-State Conditions. *Phys. Rev. Lett.* **2009**, *102*, 218103.
- (34) Grima, R. Investigating the Robustness of the Classical Enzyme Kinetic Equations in Small Intracellular Compartments. *BMC Syst. Biol.* **2009**, *3*, 101.
- (35) Grima, R.; Thomas, P.; Straube, A. V. How Accurate are the Nonlinear Chemical Fokker-Planck and Chemical Langevin Equations? *J. Chem. Phys.* **2011**, *135*, 084103.
- (36) Thomas, P.; Straube, A. V.; Grima, R. The Slow-Scale Linear Noise Approximation: An Accurate, Reduced Stochastic Description of Biochemical Networks Under Timescale Separation Conditions. *BMC Syst. Biol.* **2012**, *6*, 39.
- (37) Thomas, P.; Straube, A. V.; Grima, R. Stochastic Theory of Large-Scale Enzyme-Reaction Networks: Finite Copy Number Corrections to Rate Equation Models. *J. Chem. Phys.* **2010**, *133*, 195101.
- (38) Ramaswamy, R.; González-Segredo, N.; Sbalzarini, I. F.; Grima, R. Discreteness-Induced Concentration Inversion in Mesoscopic Chemical Systems. *Nat. Commun.* **2012**, *3*, 779.
- (39) McKane, A. J.; Nagy, J. D.; Newman, T. J.; Stefanini, M. O. Amplified Biochemical Oscillations in Cellular Systems. *J. Stat. Phys.* **2007**, *128*, 165–191.
- (40) Thomas, P.; Straube, A. V.; Timmer, J.; Fleck, C.; Grima, R. Signatures of Nonlinearity in Single Cell Noise-Induced Oscillations. *J. Theor. Biol.* **2013**, *335*, 222–234.
- (41) Ramaswamy, R.; Sbalzarini, I. F. Intrinsic Noise Alters the Frequency Spectrum of Mesoscopic Oscillatory Chemical Reaction Systems. *Sci. Rep.* **2011**, *1*, 154.
- (42) Fidleo, M.; Lavecchia, R. Kinetic Study of Enzymatic Urea Hydrolysis in the pH Range 4–9. *Chem. Biochem. Eng. Q.* **2003**, *17*, 311–318.
- (43) Krajewska, B. Ureases I. Functional, Catalytic and Kinetic Properties: A Review. *J. Mol. Catal. B: Enzym.* **2009**, *59*, 9–21.
- (44) Eigen, M. Proton Transfer, Acid-Base Catalysis, and Enzymatic Hydrolysis. Part I: Elementary Processes. *Angew. Chem., Int. Ed. Engl.* **1964**, *3*, 1–19.
- (45) Winkelmann, S.; Schütte, C. The Spatiotemporal Master Equation: Approximation of Reaction-Diffusion Dynamics via Markov State Modeling. *J. Chem. Phys.* **2016**, *145*, 214107.
- (46) Winkelmann, S.; Zonker, J.; Schütte, C.; Conrad, N. D. Mathematical Modeling of Spatio-Temporal Population Dynamics and Application to Epidemic Spreading. *Math. Biosci.* **2021**, *336*, 108619.
- (47) Gillespie, D. T. Exact Stochastic Simulation of Coupled Chemical Reactions. *J. Phys. Chem.* **1977**, *81*, 2340–2361.
- (48) Gillespie, D. T.; Hellander, A.; Petzold, L. R. Perspective: Stochastic Algorithms for Chemical Kinetics. *J. Chem. Phys.* **2013**, *138*, 170901.
- (49) Segel, L. A.; Slemrod, M. The Quasi-Steady-State Assumption: A Case Study in Perturbation. *SIAM Rev.* **1989**, *31*, 446–477.
- (50) Benoit, É.; Callot, J. L.; Diener, F.; Diener, M. Chasse au Canard. *Collect. Math.* **1981**, *31*, 37–119.
- (51) Desroches, M.; Jeffrey, M. R. Canards and Curvature: The ‘Smallness of ϵ ’ in Slow-Fast Dynamics. *Proc. R. Soc. London, Ser. A* **2011**, *467*, 2404–2421.
- (52) Hirsch, M. W.; Smale, S.; Devaney, R. L. *Differential Equations, Dynamical Systems, and an Introduction to Chaos*; Academic Press: Boston, MA, 2013; DOI: 10.1016/C2009-0-61160-0.
- (53) Pikovsky, A.; Rosenblum, M.; Kurths, J. *Synchronization: A Universal Concept in Nonlinear Sciences*; Cambridge University Press: Cambridge, U.K., 2001; DOI: 10.1017/CBO9780511755743.
- (54) Budroni, M. A.; Torbensen, K.; Ristori, S.; Abou-Hassan, A.; Rossi, F. Membrane Structure Drives Synchronization Patterns in Arrays of Diffusively Coupled Self-Oscillating Droplets. *J. Phys. Chem. Lett.* **2020**, *11*, 2014–2020.
- (55) Budroni, M. A.; Pagano, G.; Conte, D.; Paternoster, B.; D’ambrosio, R.; Ristori, S.; Abou-Hassan, A.; Rossi, F. Synchronization Scenarios Induced by Delayed Communication in Arrays of Diffusively Coupled Autonomous Chemical Oscillators. *Phys. Chem. Chem. Phys.* **2021**, *23*, 17606–17615.